Transformation Multithermotics: Controlling Radiation and Conduction Simultaneously

Liujun Xu, Gaole Dai, and Jiping Huang[*]

Department of Physics, State Key Laboratory of Surface Physics, and Key Laboratory of Micro and Nano Photonic Structures (MOE), Fudan University, Shanghai 200438, China

Any object with nonzero temperature emits thermal radiation described by the Stefan-Boltzmann law, and hence, thermal conduction is always accompanied by thermal radiation. Although a transformation theory has been proposed to control thermal conduction, a transformation theory has not yet been put forward to manipulate thermal radiation, let alone the thermal coupling between radiation and conduction (herein called multithermotics). To solve the problem, we establish the theory of transformation multithermotics to control radiation and conduction simultaneously. As model applications, we also design three devices with functions of cloaking, concentrating, and rotating. These devices are confirmed by transient finite-element simulations. As experimental suggestions, we further design transformation media with two homogeneous and isotropic materials to simplify fabrication. Our results provide general hints to multithermal management, and have potential applications in infrared camouflaging, solar-energy utilizing, etc.

I. INTRODUCTION

Heat energy is one of the most common forms of energy in nature. As one of the basic modes of heat transfer, thermal conduction has attracted wide research interest whether at the nanoscale [1–5] or at the macroscale [6–8]. Meanwhile, thermal radiation always exists together with thermal conduction because any object with nonzero temperature emits thermal radiation described by the Stefan-Boltzmann law. Therefore, the thermal coupling between radiation and conduction is ubiquitous in nature. In particular, thermal radiation must be taken into consideration when discussing the heat transfer in aerogels [9–11] because thermal radiation largely affects the insulation effect of aerogels at high temperature.

Transformation theory, bridging space transformation and material transformation, was originally proposed to control electromagnetic fields [12]. As a fundamental method, transformation theory has been extended from electromagnetic waves [12] to matter waves [13], water waves [14–16], and even to diffusion systems such as thermal conduction [6–8], electrical conduction [17], and fluid dynamics [18,19].

However, the existing theory of transformation optics [12] cannot be directly used to handle thermal radiation because the radiative model of participating media such as aerogels is dealt with the Rosseland diffusion

approximation [9–11]. Therefore, it is necessary to establish another transformation theory to handle the thermal coupling between radiation and conduction (herein called transformation multithermotics).

For this purpose, we study the Rosseland diffusion approximation [20], derived from the Stefan-Boltzmann law, to deal with thermal radiation. Such an approximation supposes that the mean free path of photons is far smaller than system size. Therefore, the propagation of thermal radiation can be regarded as the diffusion of photons. Based on the approximation, we establish the theory of transformation multithermotics [Fig. 1(a)]. As model applications, we further design three devices with functions of cloaking, concentrating, and rotating. Cloaking [Fig. 1(b)] can protect inside objects from being discovered by infrared detection; concentrating [Fig. 1(c)] can enhance the intensity of local heat flux; and rotating [Fig. 1(d)] can control the direction of local heat flux. Since transformation media are inhomogeneous and anisotropic, we also use layered structures composed of two homogeneous and isotropic materials to simplify fabrication.

II. ESTABLISHING THE THEORY OF TRANSFORMATION MULTITHERMOTICS

We consider a transient process of heat transfer with the thermal coupling between radiation and conduction. Radiative flux $\mathbf{J}_{\mathrm{rad}}$ $\left(= -16/3\boldsymbol{\beta}^{-1}\mathbf{n}^2\sigma T^3 \cdot \nabla T\right)$ is given by the Rosseland diffusion approximation [20], where $\boldsymbol{\beta}$
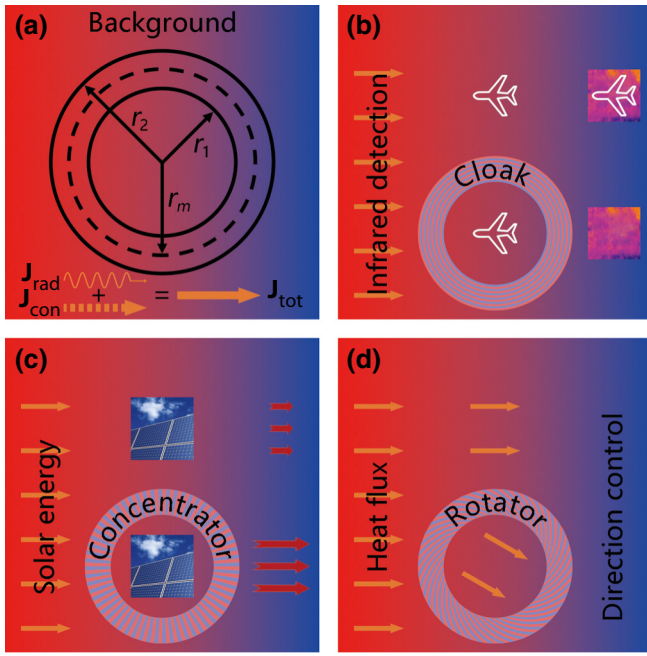
―――――
[*]jphuang@fudan.edu.cn

FIG. 1. Schematic graphs. Color surfaces denote thermal fields. (a) Illustration of multithermotics where the wavy arrow, dashed arrow, and solid arrow represent radiative flux, conductive flux, and total flux, respectively. (b) Illustration of cloaking, which can protect inside objects (such as a plane) from being discovered by infrared detection. (c) Illustration of concentrating, which can help to enhance the utilization efficiency of solar energy. (d) Illustration of rotating, which can realize the direction control of local heat flux.

is the Rosseland mean attenuation coefficient, $\mathbf{n}$ is relative refractive index, σ is the Stefan-Boltzmann constant $\left(= 5.67 \times 10^{-8}\ \mathrm{W\,m^{-2}\,K^{-4}}\right)$, and T denotes temperature. Conductive flux $\mathbf{J}_{\mathrm{con}}$ $\left(= -\boldsymbol{\kappa} \cdot \nabla T\right)$ is determined by the Fourier law, where $\boldsymbol{\kappa}$ is thermal conductivity. In what follows, we start form proving the form-invariance of the dominant equation of multithermotics, and then, derive the transformation rules, which are the key to transformation multithermotics.

If heat transfer is passive, the dominant equation of multithermotics becomes

$$\rho C \partial T / \partial t + \nabla \cdot (\mathbf{J}_{\mathrm{rad}} + \mathbf{J}_{\mathrm{con}}) = 0, \qquad (1)$$

where ρ and C are the density and heat capacity of participating media, respectively.

We can check that Eq. (1) keeps its form-invariance under a space transformation, namely from a curvilinear space X to a physical space X', which is determined by the Jacobian transformation matrix $\mathbf{A}$. The proofs are as follows.

For this purpose, we write down the component form of Eq. (1). In a curvilinear space with a contravariant basis $\{\mathbf{g}^u, \mathbf{g}^v, \mathbf{g}^w\}$, a covariant basis $\left\{\mathbf{g}_u, \mathbf{g}_v, \mathbf{g}_w\right\}$, and

corresponding contravariant components $\{x^u, x^v, x^w\}$, the radiative term can be rewritten as

$$\nabla \cdot (\boldsymbol{\alpha} T^3 \cdot \nabla T) = \mathbf{g}^w \cdot \frac{\partial}{\partial x^w} \left(\alpha^{uv} T^3 \mathbf{g}_u \otimes \mathbf{g}_v \cdot \mathbf{g}^l \frac{\partial T}{\partial x^l} \right)$$

$$= \mathbf{g}^w \cdot \frac{\partial}{\partial x^w} \left(\alpha^{uv} T^3 \mathbf{g}_u \frac{\partial T}{\partial x^v} \right)$$

$$= \frac{\partial \alpha^{uv} T^3}{\partial x^u} \frac{\partial T}{\partial x^v} + \frac{\partial^2 T}{\partial x^u \partial x^v} \alpha^{uv} T^3$$

$$+ \mathbf{g}^w \cdot \frac{\partial \mathbf{g}_u}{\partial x^w} \left(\alpha^{uv} T^3 \frac{\partial T}{\partial x^v} \right)$$

$$= \partial_u \left(\alpha^{uv} T^3 \partial_v T \right) + \Gamma^w_{wu} \alpha^{uv} T^3 \partial_v T$$

$$= \partial_u \left(\alpha^{uv} T^3 \partial_v T \right) + \frac{1}{\sqrt{g}} (\partial_u \sqrt{g}) \alpha^{uv} T^3 \partial_v T$$

$$= \frac{1}{\sqrt{g}} \partial_u \left(\sqrt{g} \alpha^{uv} T^3 \partial_v T \right), \qquad (2)$$

where $\boldsymbol{\alpha}$ $\left(= 16/3 \boldsymbol{\beta}^{-1} \mathbf{n}^2 \sigma\right)$ can be regarded as radiative coefficient, and g is the determinant of the matrix with components $g_{ij} = \mathbf{g}_u \cdot \mathbf{g}_v$. The Christoffel symbol is defined as $\Gamma^w_{vu} = \partial \mathbf{g}_u / \partial x^v \cdot \mathbf{g}^w$, thus resulting in $\Gamma^w_{wu} = \left(\partial_u \sqrt{g}\right) / \sqrt{g}$. Similarly, the conductive term can also be rewritten as

$$\nabla \cdot (\boldsymbol{\kappa} \cdot \nabla T) = \frac{1}{\sqrt{g}} \partial_u \left(\sqrt{g} \kappa^{uv} \partial_v T \right). \qquad (3)$$

Then, Eq. (1) can be rewritten into the component form as

$$\sqrt{g} \rho C \partial_t T - \partial_u \left[\sqrt{g} \left(\alpha^{uv} T^3 + \kappa^{uv} \right) \partial_v T \right] = 0, \qquad (4)$$

which is expressed in the curvilinear space. So far, we prove the form-invariance of Eq. (1). Then, we should rewrite it in the physical space to get the transformation rules of material properties, which is usually written in the Cartesian coordinate system $\left\{x^{u'}, x^{v'}, x^{w'}\right\}$,

$$\sqrt{g} \rho C \partial_t T - \partial_{u'} \frac{\partial x^{u'}}{\partial x^u} \left[\sqrt{g} \left(\alpha^{uv} T^3 + \kappa^{uv} \right) \frac{\partial x^{v'}}{\partial x^v} \partial_{v'} T \right] = 0, \qquad (5)$$

where $\partial x^{u'} / \partial x^u$ and $\partial x^{v'} / \partial x^v$ are just the components of the Jacobian transformation matrix $\mathbf{A}$, and $g = \det^{-2} \mathbf{A}$. We replace space transformation with material transformation,

$$\frac{\rho C}{\det \mathbf{A}} \partial_t T - \partial_{u'} \left[\left(\frac{A^{u'}_u \alpha^{uv} A^{v'}_v}{\det \mathbf{A}} T^3 + \frac{A^{u'}_u \kappa^{uv} A^{v'}_v}{\det \mathbf{A}} \right) \partial_{v'} T \right] = 0. \qquad (6)$$

Therefore, transformation rules can be expressed as

$$(\rho C)' = \rho_0 C_0 / \det \mathbf{A},$$
$$\boldsymbol{\alpha}' = \mathbf{A}\boldsymbol{\alpha}_0 \mathbf{A}^\tau / \det \mathbf{A}, \tag{7}$$
$$\boldsymbol{\kappa}' = \mathbf{A}\boldsymbol{\kappa}_0 \mathbf{A}^\tau / \det \mathbf{A},$$

where ρ_0, C_0, $\boldsymbol{\alpha}_0$, and $\boldsymbol{\kappa}_0$ are, respectively, the density, heat capacity, radiative coefficient, and thermal conductivity of the background. $\mathbf{A}^\tau$ denotes the transpose of $\mathbf{A}$. Thermal radiation is dominated by radiative coefficient, which is composed of two physical quantities, namely the Rosseland mean attenuation coefficient and relative refractive index. For the consideration of variables control, we set the relative refractive indexes of all regions to 1 and discuss the transformation rule of the Rosseland mean attenuation coefficient. Certainly, the present theory can also be applied to other relative refraction indexes as long as the transformation requirement of radiative coefficient is satisfied. Then, Eq. (7) can be simplified as

$$(\rho C)' = \rho_0 C_0 / \det \mathbf{A},$$
$$\mathbf{n}' = \mathbf{n}_0,$$
$$\boldsymbol{\beta}' = \mathbf{A}^{-\tau} \boldsymbol{\beta}_0 \mathbf{A}^{-1} \det \mathbf{A}, \tag{8}$$
$$\boldsymbol{\kappa}' = \mathbf{A}\boldsymbol{\kappa}_0 \mathbf{A}^\tau / \det \mathbf{A}.$$

Equation (7) or (8) is the key to transformation multithermotics. We use Eq. (8) for brevity when performing finite-element simulations.

III. USING THE THEORY TO DESIGN CLOAKING, CONCENTRATING, AND ROTATING

Since transformation multithermotics does not restrict space dimensions, we discuss a two-dimensional system to design cloaking, concentrating, and rotating without loss of generality.

The space transformation of cloaking is to compress a circular region ($r < r_1$) from the center into a shell ($r_1 < r < r_2$), which can be expressed as

$$r' = (r_2 - r_1)\, r/r_2 + r_1,$$
$$\theta' = \theta, \tag{9}$$

where r_1 and r_2 are the inner and outer radii of the shell, and $0 < r < r_2$ except for additional statements.

The space transformation of concentrating is firstly to compress a lager circular region ($r < r_m$) into a small one ($r < r_1$). Secondly, the small shell ($r_m < r < r_2$) is stretched into a large one ($r_1 < r < r_2$). The two steps can

be concluded as

$$r' = r_1 r/r_m \quad \text{for } r < r_m,$$
$$r' = [(r_2 - r_1)\, r + (r_1 - r_m)\, r_2] / (r_2 - r_m)$$
$$\quad \text{for } r_m < r < r_2, \tag{10}$$
$$\theta' = \theta,$$

where r_m determined the concentrating ratio.

The space transformation of rotating is to rotate the core ($r < r_1$) with angle θ_0 and rotate the shell ($r_1 < r < r_2$) as

$$r' = r,$$
$$\theta' = \theta + \theta_0 \quad \text{for } r < r_1, \tag{11}$$
$$\theta' = \theta + \theta_0\, (r - r_2) / (r_1 - r_2) \quad \text{for } r_1 < r < r_2,$$

where θ_0 is the rotation angle.

The Jacobian transformation matrix of Eqs. (9)–(11) can be calculated by

$$\mathbf{A} = \begin{pmatrix} \partial r'/\partial r & \partial r'/ (r\partial\theta) \\ r'\partial\theta'/\partial r & r'\partial\theta'/ (r\partial\theta) \end{pmatrix}. \tag{12}$$

IV. CONFIRMING THE THEORY WITH TRANSIENT FINITE-ELEMENT SIMULATIONS

We further perform transient finite-element simulations with COMSOL Multiphysics [21]. In the template of "Heat Transfer with Radiation in Participating Media," the Rosseland mean attenuation coefficient is isotropic by default. Therefore, we should rewrite the heat-transfer equation with tensorial parameters in the interface with general partial differential equations.

Then, we choose three different temperature intervals to present the influence of thermal radiation. (I) 300–320 K: in this temperature interval, radiative flux is far smaller than conductive flux ($\mathbf{J}_{\mathrm{rad}} \ll \mathbf{J}_{\mathrm{con}}$) due to the low temperature. (II) 300–1000 K: in this temperature interval, as the temperature rises, thermal radiation starts influencing the temperature profile due to $\mathbf{J}_{\mathrm{rad}} \sim \mathbf{J}_{\mathrm{con}}$. (III) 300–3000 K: in this temperature interval, the temperature is already very high, and hence, thermal radiation becomes the dominant effect because of $\mathbf{J}_{\mathrm{rad}} \gg \mathbf{J}_{\mathrm{con}}$. Here, 3000 K is reasonable because carbon aerogels are reported to have tolerance up to high temperature of 3073 K [22]. We set the temperature intervals to the left and right boundaries, and the upper and lower boundaries are insulated. The initial temperature is set at 300 K. It takes about 100, 50, and 5 min for the three temperature intervals to reach steady states, respectively. The transient finite-element simulations of cloaking, concentrating, and rotating are presented in Figs. 2–4, respectively.

The cloaking parameters are set as required by Eq. (9). We also set the boundary at $r = r_1$ to be insulated. One purpose is to make the cloaking effect clear because any object
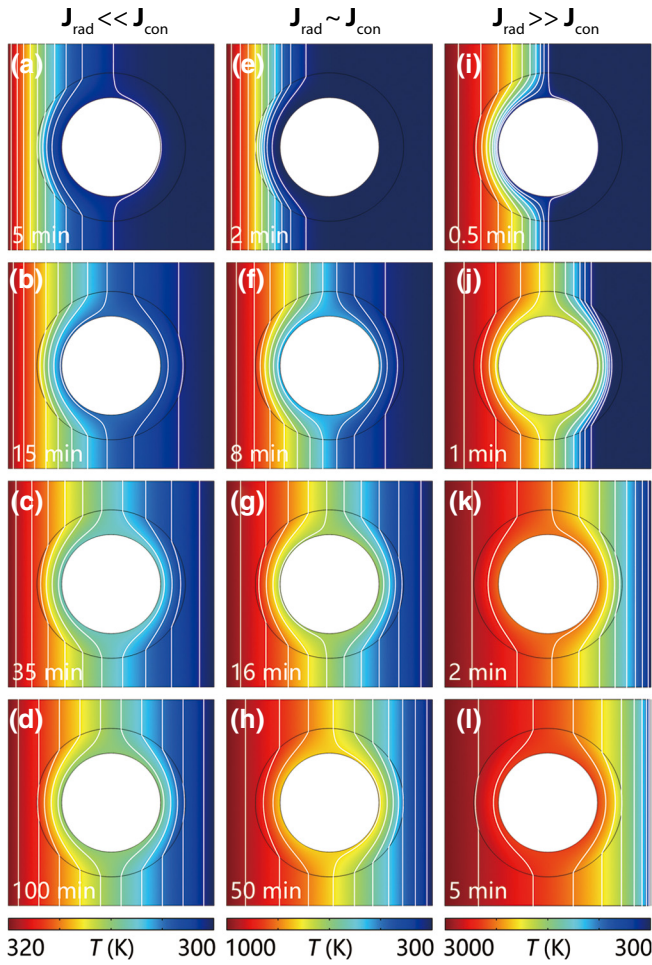
FIG. 2. Simulations of cloaking. White lines represent isotherms, and rainbow surfaces denote temperature distributions. The size is 10×10 cm^2, $r_1 = 2.4$ cm, $r_2 = 3.6$ cm, and the background parameters are $\rho_0 C_0 = 10^6$ Jm^{-3}K^{-1}, $\mathbf{n}_0 = 1$, $\beta_0 = 100$ m^{-1}, and $\kappa_0 = 1$ Wm^{-1}K^{-1} throughout this work. The shell parameters are $\mathbf{A} = \text{diag}\left\{(r_2 - r_1)/r_2, [(r_2 - r_1)/r_2][r'/(r' - r_1)]\right\}$, $(\rho C)' = [r_2/(r_2 - r_1)]^2 [(r' - r_1)/r'] \times 10^6$ Jm^{-3}K^{-1}, $\mathbf{n}' = 1$, $\beta' = \text{diag}\left[r'/(r' - r_1), (r' - r_1)/r'\right] \times 100$ m^{-1}, and $\kappa' = \text{diag}\left[(r' - r_1)/r', r'/(r' - r_1)\right]$ Wm^{-1}K^{-1}. The evolutions over time are demonstrated in (a)–(d), (e)–(h), and (i)–(l), with three different temperature intervals.

FIG. 3. Simulations of concentrating. Background parameters are unchanged. The shell parameters are $\mathbf{A} = \text{diag}\left\{(r_2 - r_1)/(r_2 - r_m), (r_2 - r_1) r'/[(r_2 - r_m) r' - (r_1 - r_m) r_2]\right\}$, $(\rho C)' = [(r_2 - r_m)^2 r' - (r_2 - r_m)(r_1 - r_m) r_2]/[(r_2 - r_1)^2 r'] \times 10^6$ Jm^{-3}K^{-1}, $\mathbf{n}' = 1$, $\beta' = \text{diag}\{(r_2 - r_m) r'/[(r_2 - r_m) r' - (r_1 - r_m) r_2], [(r_2 - r_m) r' - (r_1 - r_m) r_2]/[(r_2 - r_m) r']\} \times 100$ m^{-1}, and $\kappa' = \text{diag}\{[(r_2 - r_m) r' - (r_1 - r_m) r_2]/[(r_2 - r_m) r'], (r_2 - r_m) r'/[(r_2 - r_m) r' - (r_1 - r_m) r_2]\}$ Wm^{-1}K^{-1} with $r_m = 3.2$ cm.

can be placed in the white regions presented in Fig. 2. The other purpose is to avoid the errors resulting form the singular parameters of cloaking. The evolutions of temperature profiles over time with three different temperature intervals are presented in Figs. 2(a)–2(d), Figs. 2(e)–2(h), and Figs. 2(i)–2(l), respectively. We can find that the temperature profiles of the background are never distorted over time, indicating the excellent cloaking performance.

The concentrating parameters are set as required by Eq. (10). Figures 3(a)–3(d), Figs. 3(e)–3(h), and Figs. 3(i)–3(l) show the evolutions of temperature profiles
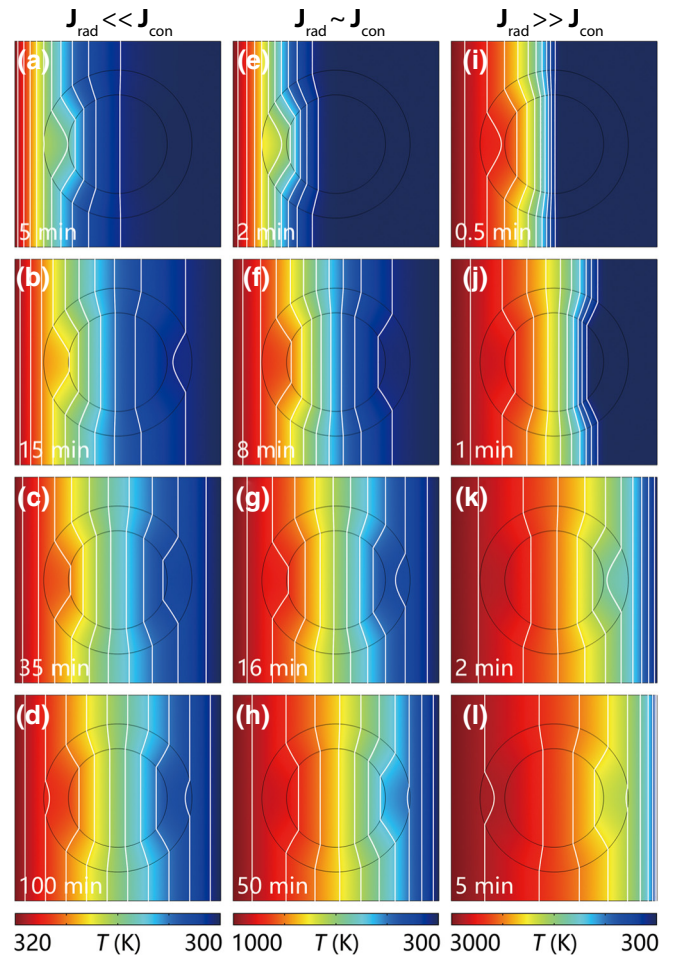
over time with three preset temperature intervals, respectively. Clearly, the isotherms in the center are concentrated, and meanwhile, those in the background are not distorted, which validate the concentrating effect.

The rotating parameters are set as required by Eq. (11). We set the rotation angle to be $\theta_0 = \pi/6$ to realize the direction control of local heat flux. Figures 4(a)–4(d), Figs. 4(e)–4(h), and Figs. 4(i)–4(l) illustrate the evolutions of temperature profiles over time with different temperature intervals. In the regions $r < r_1$, the high temperature appears at the left-top corner, indicating that the direction of heat flux is changed. Therefore, the rotating effect is achieved.
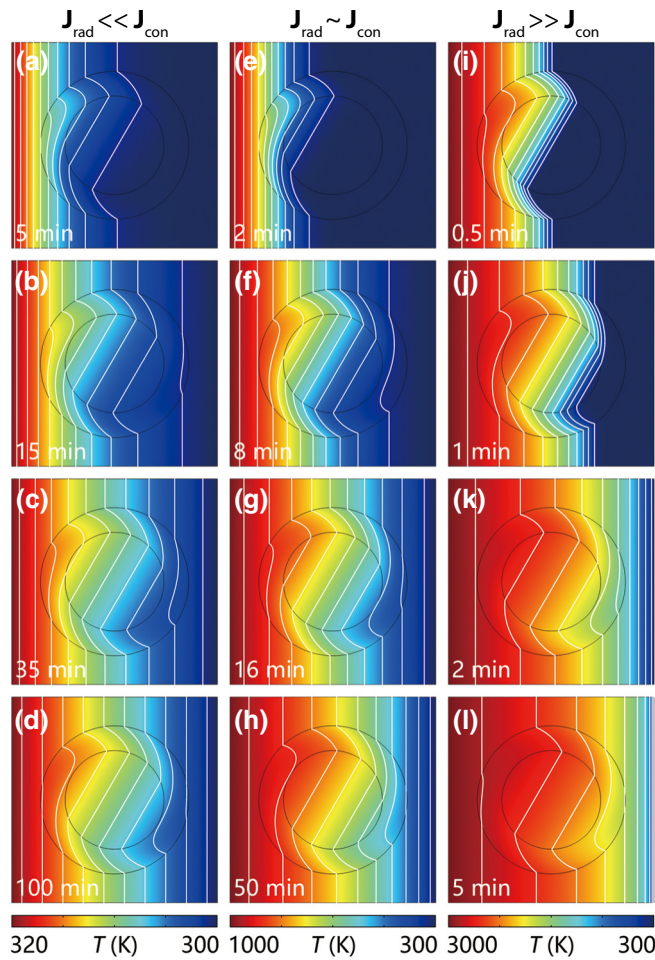
FIG. 4. Simulations of rotating. The background parameters are unchanged. The shell parameters are $\mathbf{A} = \{(1, 0), [\theta_0 r'/(r_1 - r_2), 1]\}$, $(\rho C)' = 10^6$ $\mathrm{J\,m^{-3}\,K^{-1}}$, $\mathbf{n}' = 1$, $\boldsymbol{\beta}' = (\{[\theta_0 r'/(r_1 - r_2)]^2 + 1, (-\theta_0 r')/(r_1 - r_2)\}, [(-\theta_0 r')/(r_1 - r_2), 1]) \times 100\,\mathrm{m^{-1}}$, and $\boldsymbol{\kappa}' = ([1, \theta_0 r'/(r_1 - r_2)], \{\theta_0 r'/(r_1 - r_2), [\theta_0 r'/(r_1 - r_2)]^2 + 1\})\,\mathrm{W\,m^{-1}\,K^{-1}}$ with $\theta_0 = \pi/6$.

V. EXPERIMENTAL SUGGESTIONS WITH HOMOGENEOUS AND ISOTROPIC MATERIALS

The parameters derived from transformation multithermotics are anisotropic (for all functions) and divergent (for only cloaking), which are difficult to obtain directly. With the physical image of series-parallel connection, we can imagine that layered structures have different properties along the directions of series connection and parallel connection. Therefore, we can resort to the layered structure [23–31] composed of two isotropic and homogeneous materials to effectively realize anisotropy. In other words, the effective parameters of layered structures are the approximation of the theoretical parameters, which are still anisotropic. Two general principles of structural effects are: (I) the more layers, the better; and (II) the bigger difference of both thermal conductivities and the Rosseland mean attenuation coefficients between material A and
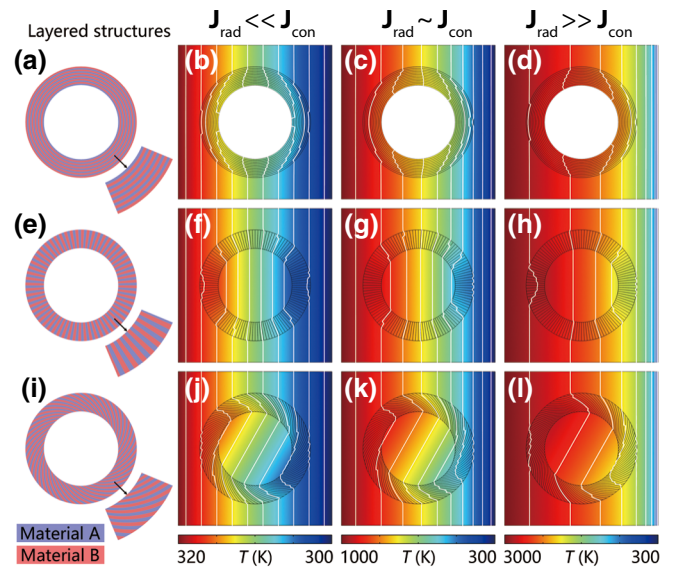

FIG. 5. Simulations of three devices with two homogeneous and isotropic materials. Material A: $\boldsymbol{\beta}_A = 800$ $\mathrm{m^{-1}}$ and $\boldsymbol{\kappa}_A = 0.125$ $\mathrm{W\,m^{-1}\,K^{-1}}$; material B: $\boldsymbol{\beta}_B = 12.5$ $\mathrm{m^{-1}}$ and $\boldsymbol{\kappa}_B = 8$ $\mathrm{W\,m^{-1}\,K^{-1}}$. (a) 12 layers with each layer having 1 mm thickness. (e) 120 layers with each layer having $3°$ flare angle. (i) 90 layers with the helical line determined by $x = r_1 \exp(s) \cos(ks)$, $y = r_1 \exp(s) \sin(ks)$, where $s \in [0, \ln(r_2/r_1)]$, and $k = 1.6$. (b)–(d), (f)–(h), and (j)–(l) show the steady results of (a), (e), and (i) with three different temperature intervals, respectively.

material B, the better. Material parameters are chosen to be around the order of aerogels. A recent study reported that the thermal conductivity of ceramic aerogels can be as low as 0.0024 $\mathrm{W\,m^{-1}\,K^{-1}}$ [32]. Therefore, the material foundation is well established. The layered structures of cloaking, concentrating, and rotating are demonstrated in Figs. 5(a), 5(e), and 5(i), respectively. The corresponding steady results are shown in Figs. 5(b)–5(d), 5(f)–5(h), and 5(j)–5(l) with three different temperature intervals, respectively. These results indicate the good performance of designed structures.

VI. DISCUSSION AND CONCLUSION

Transformation multithermotics is exact and robust with other conditions such as complex shapes and nonuniform thermal fields. Physically speaking, this is because we only transform space or material, which does not restrict other conditions.

The present establishment of transformation multithermotics benefits from the diffusive behavior of photons in optically thick media. Therefore, thermal radiation in this work is essentially a far-field effect. Certainly, it is also promising to extend transformation multithermotics to other radiative models [33], such as considering heat flux

due to photons or other heat carriers both in near fields and far fields [34–42].

In summary, we establish the theory of transformation multithermotics with the Rosseland diffusion approximation, and designed three devices with functions of cloaking, concentrating, and rotating with transformation media. We also simplify the fabrication of transformation media with layered structures, which require only two homogenous and isotropic materials. The proposed theory and devices indicate the exotic manipulations of multithermotics. These results have applications in thermal camouflaging [43–49], solar-energy utilizing [50–53], etc. This work also provides hints to nonlinear thermotics [54,55] because thermal radiation is featured by T^3 temperature dependence, which is an excellent candidate of thermally responsive metamaterials [56,57].

[1] B. W. Li, L. Wang, and G. Casati, Thermal Diode: Rectification of Heat Flux, Phys. Rev. Lett. **93,** 184301 (2004).

[2] J. Ren, P. Hanggi, and B. W. Li, Berry-Phase-Induced Heat Pumping and its Impact on the Fluctuation Theorem, Phys. Rev. Lett. **104,** 170601 (2010).

[3] J. Ren, S. Liu, and B. W. Li, Geometric Heat Flux for Classical Thermal Transport in Interacting Open Systems, Phys. Rev. Lett. **108,** 210603 (2012).

[4] N. B. Li, J. Ren, L. Wang, G. Zhang, P. Hanggi, and B. W. Li, Colloquium: Phononics: Manipulating heat flow with electronic analogs and beyond, Rev. Mod. Phys. **84,** 1045 (2012).

[5] H. Bao, J. Chen, X. K. Gu, and B. Y. Cao, A review of simulation methods in micro/nanoscale heat conduction, ES Energy Environ. **1,** 16 (2018).

[6] C. Z. Fan, Y. Gao, and J. P. Huang, Shaped graded materials with an apparent negative thermal conductivity, Appl. Phys. Lett. **92,** 251907 (2008).

[7] T. Y. Chen, C. N. Weng, and J. S. Chen, Cloak for curvilinearly anisotropic media in conduction, Appl. Phys. Lett. **93,** 114103 (2008).

[8] Y. Li, X. Y. Shen, Z. H. Wu, J. Y. Huang, Y. X. Chen, Y. S. Ni, and J. P. Huang, Temperature-Dependent Transformation Thermotics: From Switchable Thermal Cloaks to Macroscopic Thermal Diodes, Phys. Rev. Lett. **115,** 195503 (2015).

[9] X. Lu, M. C. Arduini-Schuster, J. Kuhn, O. Nilsson, J. Fricke, and R. W. Pekala, Thermal conductivity of monolithic organic aerogels, Science **255,** 971 (1992).

[10] U. Heinemann, R. Caps, and J. Fricke, Radiation conduction interaction: An investigation on silica aerogels, Int. J. Heat Mass Transfer **39,** 2115 (1996).

[11] H. Maleki, Recent advances in aerogels for environmental remediation applications: A review, Chem. Eng. J. **300,** 98 (2016).

[12] J. B. Pendry, D. Schurig, and D. R. Smith, Controlling electromagnetic fields, Science **312,** 1780 (2006).

[13] S. Zhang, D. A. Genov, C. Sun, and X. Zhang, Cloaking of Matter Waves, Phys. Rev. Lett. **100,** 123002 (2008).

[14] Z. Y. Wang, C. Y. Li, R. Zatianina, P. Zhang, and Y. Q. Zhang, Carpet cloak for water waves, Phys. Rev. E **96,** 053107 (2017).

[15] C. Y. Li, L. Xu, L. L. Zhu, S. Y. Zou, Q. H. Liu, Z. Y. Wang, and H. Y. Chen, Concentrators for Water Waves, Phys. Rev. Lett. **121,** 104501 (2018).

[16] S. Y. Zou, Y. D. Xu, R. Zatianina, C. Y. Li, X. Liang, L. L. Zhu, Y. Q. Zhang, G. H. Liu, Q. H. Liu, H. Y. Chen, and Z. Y. Wang, Broadband Waveguide Cloak for Water Waves, Phys. Rev. Lett. **123,** 074501 (2019).

[17] F. Yang, Z. L. Mei, T. Y. Jin, and T. J. Cui, DC Electric Invisibility Cloak, Phys. Rev. Lett. **109,** 053902 (2012).

[18] Y. A. Urzhumov and D. R. Smith, Fluid Flow Control with Transformation Media, Phys. Rev. Lett. **107,** 074501 (2011).

[19] J. Park, J. R. Youn, and Y. S. Song, Hydrodynamic Metamaterial Cloak for Drag-Free Flow, Phys. Rev. Lett. **123,** 074502 (2019).

[20] S. Rosseland, *Theoretical Astrophysics* (Oxford Univ. Press, Clarendon, London and New York, 1936).

[21] http://www.comsol.com/.

[22] Y. Hanzawa, H. Hatori, N. Yoshizawa, and Y. Yamada, Structural changes in carbon aerogels with high temperature treatment, Carbon **40,** 575 (2002).

[23] S. Narayana and Y. Sato, Heat Flux Manipulation with Engineered Thermal Materials, Phys. Rev. Lett. **108,** 214303 (2012).

[24] H. Y. Xu, X. H. Shi, F. Gao, H. D. Sun, and B. L. Zhang, Ultrathin Three-Dimensional Thermal Cloak, Phys. Rev. Lett. **112,** 054301 (2014).

[25] T. C. Han, X. Bai, D. L. Gao, J. T. L. Thong, B. W. Li, and C. W. Qiu, Experimental Demonstration of a Bilayer Thermal Cloak, Phys. Rev. Lett. **112,** 054302 (2014).

[26] Y. G. Ma, Y. C. Liu, M. Raza, Y. D. Wang, and S. L. He, Experimental Demonstration of a Multiphysics Cloak: Manipulating Heat Flux and Electric Current Simultaneously, Phys. Rev. Lett. **113,** 205501 (2014).

[27] T. C. Han, X. Bai, J. T. L. Thong, B. W. Li, and C. W. Qiu, Full control and manipulation of heat signatures: Cloaking, camouflage and thermal metamaterials, Adv. Mater. **26,** 1731 (2014).

[28] T. Y. Chen, C. N. Weng, and Y. L. Tsai, Materials with constant anisotropic conductivity as a thermal cloak or concentrator, J. Appl. Phys. **117,** 054904 (2015).

[29] T. C. Han, P. Yang, Y. Li, D. Y. Lei, B. W. Li, K. Hippalgaonkar, and C. W. Qiu, Full-parameter omnidirectional thermal metadevices of anisotropic geometry, Adv. Mater. **30,** 1804019 (2018).

[30] Y. Li, K. J. Zhu, Y. G. Peng, W. Li, T. Z. Yang, H. X. Xu, H. Chen, X. F. Zhu, S. H. Fan, and C. W. Qiu, Thermal metadevice in analogue of zero-index photonics, Nat. Mater. **18,** 48 (2019).

[31] L. J. Xu, S. Yang, and J. P. Huang, Passive Metashells with Adaptive Thermal Conductivities: Chameleonlike

Behavior and its Origin, Phys. Rev. Appl. **11,** 054071 (2019).

[32] X. Xu *et al.*, Double-negative-index ceramic aerogels for thermal superinsulation, Science **363,** 723 (2019).

[33] J. R. Howell, M. P. Menguc, and R. Siegel, *Thermal Radiation Heat Transfer* (CRC Press, Boca Raton, London, New York, 2016), 6th ed.

[34] P. Ben-Abdallah and S. A. Biehs, Near-Field Thermal Transistor, Phys. Rev. Lett. **112,** 044301 (2014).

[35] V. Kubytskyi, S. A. Biehs, and P. Ben-Abdallah, Radiative Bistability and Thermal Memory, Phys. Rev. Lett. **113,** 074301 (2014).

[36] S. A. Dyakov, J. Dai, and M. Yan, Thermal radiation dynamics in two parallel plates: The role of near field, Phys. Rev. B **90,** 045414 (2014).

[37] S. A. Dyakov, J. Dai, M. Yan, and M. Qiu, Near field thermal memory based on radiative phase bistability of VO$_2$, J. Phys. D: Appl. Phys. **48,** 305104 (2015).

[38] Z. Y. Li, Optics and photonics at nanoscale: Principles and perspectives, EPL **110,** 1 (2015).

[39] R. Messina, W. L. Jin, and A. W. Rodriguez, Exact formulas for radiative heat transfer between planar bodies under arbitrary temperature profiles: Modified asymptotics and sign-flip transitions, Phys. Rev. B **94,** 205438 (2016).

[40] V. Fernandez-Hurtado, F. J. Garcia-Vidal, S. F. Fan, and J. C. Cuevas, Enhancing Near-Field Radiative Heat Transfer with Si-Based Metasurfaces, Phys. Rev. Lett. **118,** 203901 (2017).

[41] M. Ghashami, H. Y. Geng, T. Kim, N. Iacopino, S. K. Cho, and K. Park, Precision Measurement of Phonon-Polaritonic Near-Field Energy Transfer between Macroscale Planar Structures under Large Thermal Gradients, Phys. Rev. Lett. **120,** 175901 (2018).

[42] G. T. Papadakis, B. Zhao, S. Buddhiraju, and S. H. Fan, Gate-tunable near-field heat transfer, ACS Photonics **6,** 709 (2019).

[43] T. Z. Yang, X. Bai, D. L. Gao, L. Z. Wu, B. W. Li, J. T. L. Thong, and C. W. Qiu, Invisible sensors: Simultaneous sensing and camouflaging in multiphysical fields, Adv. Mater. **27,** 7752 (2015).

[44] Y. Li, X. Bai, T. Z. Yang, H. Luo, and C. W. Qiu, Structured thermal surface for radiative camouflage, Nat. Commun. **9,** 273 (2018).

[45] R. Hu, S. L. Zhou, Y. Li, D. Y. Lei, X. B. Luo, and C. W. Qiu, Illusion thermotics, Adv. Mater. **30,** 1707237 (2018).

[46] S. L. Zhou, R. Hu, and X. B. Luo, Thermal illusion with twinborn-like heat signatures, Int. J. Heat Mass Transfer **127,** 607 (2018).

[47] R. Hu, S. Y. Huang, M. Wang, X. L. Luo, J. Shiomi, and C. W. Qiu, Encrypted thermal printing with regionalization transformation, Adv. Mater. **31,** 1807849 (2019).

[48] L. J. Xu, S. Yang, and J. P. Huang, Thermal Transparency Induced by Periodic Interparticle Interaction, Phys. Rev. Appl. **11,** 034056 (2019).

[49] J. X. Li, Y. Li, T. L. Li, W. Y. Wang, L. Q. Li, and C. W. Qiu, Doublet Thermal Metadevice, Phys. Rev. Appl. **11,** 044021 (2019).

[50] Y. Tian and C. Y. Zhao, A review of solar collectors and thermal energy storage in solar thermal applications, Appl. Energy **104,** 538 (2013).

[51] A. P. Raman, M. A. Anoma, L. X. Zhu, E. Rephaeli, and S. H. Fan, Passive radiative cooling below ambient air temperature under direct sunlight, Nature **515,** 540 (2014).

[52] Y. Zhai, Y. G. Ma, S. N. David, D. L. Zhao, R. N. Lou, G. Tan, R. G. Yang, and X. B. Yin, Scalable-manufactured randomized glass-polymer hybrid metamaterial for daytime radiative cooling, Science **355,** 1062 (2017).

[53] F. Zhao, X. Y. Zhou, Y. Shi, X. Qian, M. Alexander, X. P. Zhao, S. Mendez, R. G. Yang, L. T. Qu, and G. H. Yu, Highly efficient solar vapour generation via hierarchically nanostructured gels, Nat. Nanotechnol. **13,** 489 (2018).

[54] G. L. Dai, J. Shang, R. Z. Wang, and J. P. Huang, Nonlinear thermotics: Nonlinearity enhancement and harmonic generation in thermal metasurfaces, Eur. Phys. J. B **91,** 59 (2018).

[55] S. Yang, L. J. Xu, and J. P. Huang, Metathermotics: Nonlinear thermal responses of core-shell metamaterials, Phys. Rev. E **99,** 042144 (2019).

[56] K. L. Nguyen, O. Merchiers, and P. O. Chapuis, Temperature-dependent and optimized thermal emission by spheres, Appl. Phys. Lett. **112,** 111906 (2018).

[57] S. Kang, J. Cha, K. Seo, S. Kim, Y. Cha, H. Lee, J. Park, and W. Choi, Temperature-responsive thermal metamaterials enabled by modular design of thermally tunable unit cells, Int. J. Heat Mass Transfer **130,** 469 (2019).